Proceedings of the ASME 2010 3rd Joint US-European Fluids Engineering Summer Meeting and 8th International Conference on Nanochannels, Microchannels, and Minichannels
FEDSM-ICNMM2010
August 1-5, 2010, Montreal, Canada

FEDSM-ICNMM2010-30098

FUEL SPRAY SIMULATION WITH COLLISION JETS FOR AUTOMOBILE ENGINES

Eiji Ishii
Mechanical Engineering Research Laboratory, Hitachi, Ltd.
Hitachinaka, Ibaraki, Japan

Yoshihiro Sukegawa
Hitachi Laboratory, Hitachi, Ltd.
Hitachinaka, Ibaraki, Japan

Hiroshi Yamada
Hitachi Automotive Systems, Ltd.
Isesaki, Gunma, Japan

ABSTRACT

Fuel injectors for automobile engines atomize fuel into multi-scale free surfaces: liquid films formed at the fuel-injector outlet, ligaments generated by the liquid-film breakup, and droplets generated from the ligaments within the air/fuel mixture region. We previously developed a fuel spray simulation combining the liquid-film breakup near the injector outlet with the air/fuel mixture. The liquid-film breakup was simulated by a particle method. The fuel-droplet behavior in the air/fuel mixture region was simulated by a discrete droplet model (DDM).

In this study, we applied our method to simulate fuel sprays from a fuel injector with collision jets. The simulation results were compared with the measurements— the mean diameter of droplet in spray, D_{32}, was 35 percent larger than measured D_{32}. We also studied the effects of DDM injection conditions on the spray distribution in the air/fuel mixture region— diameter distributions of injected DDM-droplets were given by the liquid-film breakup simulation, or by Nukiyama-Tanazawa's theory. The diameter distribution of droplets near the injector outlet was found to affect the spray distribution within the air/fuel mixture region, mainly around the leading edge of spray.

INTRODUCTION

To protect the Earth's environment, lower engine emissions and improved fuel efficiency have recently become more necessary in automobile engines. Fuel injectors are used for atomizing fuel into minute droplets of fuel spray, which are then injected into automobile engines. Both finely atomizing the fuel and injecting the spray into automobile engines lower engine emissions and improve fuel efficiency. Computer simulations of the fuel spray are very useful in studying the atomization and the spray form. However, the fuel-spray simulation is hard, because the fuel spray contains multi-scale free surfaces: liquid films formed at the injector outlet, ligaments generated by liquid-film breakup near the injector outlet (within a few millimeters of the injector outlet), and fuel-droplet in the air/fuel mixture region (within about 100 millimeters of the injector outlet).

The liquid-film breakup, involving the liquid films and the ligaments, has mainly been simulated with front-capturing methods (for example, volume of fluid method [1], level set method [2], and cubic interpolated propagation (CIP) method [3]) [4][5][6]. However, in these methods, free surfaces are lost due to numerical diffusion, and a long computation time is required because it is necessary to use computational grids finer than the thickness of the liquid films and ligaments. To avoid losing free surfaces, we previously developed a particle/grid hybrid method [7][8]. Both the fuel flow within the flow paths of the injector and the liquid film at the injector outlet were simulated by a grid method, namely, CIP. Furthermore, the liquid-film breakup was simulated by a particle method (moving-particle semi-implicit (MPS) method [9]). In the simulation, particles were moved as a fully Lagrangian description, which avoids free surfaces being lost due to numerical diffusion.

The fuel-droplet behavior in the air/fuel mixture region was generally simulated by a discrete droplet model (DDM) [10]; a DDM-droplet is a group of droplets injected under the same velocity, diameter, and time conditions. The DDM-droplet was defined as a sphere. The injection conditions of the DDM-droplet were defined by velocity and diameter distributions given from measurements. However, to cut the cost for

measurements, the measurements had to be replaced by the computer simulation (that is, the liquid-film breakup simulation).

In recent studies, we developed a fuel-spray simulation that combines the behaviors of the air/fuel mixture and the liquid-film breakup [11]. Figure 1 shows the simulation model used in this study. Both the fuel flows within the flow paths of the injector, the liquid film at the injector outlet, and airflow near an injector outlet were simulated by a grid method, namely, CIP. Furthermore, the liquid-film breakup near the injector outlet was simulated by the particle method, namely, MPS. The DDM injection conditions (velocity and diameter distributions of DDM-droplets) were defined by distributions of velocities and diameters that were calculated in the simulation of the liquid-film breakup. The data-sampling region was assigned within a few millimeters of the injector outlet. The airflow in the air/fuel mixture region was simulated by using the Cartesian-grid method [12] with uniform rectangular computational grids. Note that the computational grids within a complex geometry can be generated from computer-aided design (CAD) data in a few minutes.

In this study, at first, we modified the particle/grid hybrid method in our fuel spray simulation; procedure combining particle and grid methods were changed to get better numerical convergence. A simple benchmark test, dam break problem by Martine and Moyce, was used for the verification of our method. Then, we applied our method to simulate the spray from some test injector-models with a collision jet. The simulation results were qualitatively verified by comparing them with measurements; predicted droplet diameters in sprays from the test injector-models with some changes of nozzle dimensions were compared with those of measurements. It was found that the simulation predicted the relative differences of mean droplet diameters between the test injector-models, and the errors of mean droplet diameters between the simulations and measurements were less than 11 percent.

NOMENCLATURE

d	: diameter of DDM-droplet
$N^{(i)}$	: particle number density of fluid i (i = 1 or 2), integrated in radius R_e
N_0	: particle number density defined by particle-distribution at the start of computation
R	: distance between a particle and a grid
R_e	: effective range of interpolation
t	: time
u	: velocity
W	: weight function of interpolation
$\delta^{(i)}$	: distance from free surface (number of cells) within fluid i (i = 1 or 2)
μ	: viscosity
θ_{CIP}	: volume fraction of liquid calculated by CIP
ρ	: density

Subscript

CIP	: parameters related to CIP
d	: parameters related to DDM-droplet
a	: parameters related to air in air/fuel mixture simulation
MPS	: parameters related to MPS

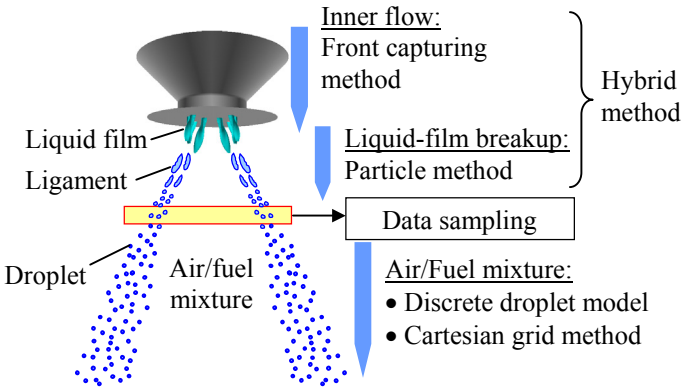

Fig. 1 Simulation model for fuel spray with air/fuel mixtrure.

FORMULATION

Liquid-film breakup simulation The liquid-film breakup was simulated with the particle/grid hybrid method [8]; liquid films, ligaments, and droplets that were smaller than the grid sizes were calculated by MPS, and other flow fields were calculated by CIP. For the particle/grid hybrid method, MPS and CIP were combined in the following three steps:

Step 1: Advection velocities are calculated from the advection equations of MPS and CIP.

Step 2: Advection velocities determined in step 1 are modified by using a weight function on the basis of a particle-number density given by MPS and a distance (defined by the number of cells shown in Fig. 3) from a free surface. The position of the free surface is defined as 0.5 of volume fraction of liquid given by CIP.

Step 3: Diffusion and source terms are calculated. After that, the Poisson equations of pressure used in both methods are solved respectively. Velocity and coordinates of particles are modified by using the pressure given by the Poisson equation in MPS.

Here, only step 2 was added to the original procedures (namely, steps 1 and 3) in MPS and CIP. In step 2, the advection velocities were modified as

$$\vec{u}^{*}_{MPS} = (1-\lambda_{MPS})\,\vec{u}_{MPS} + \lambda_{MPS}\,\vec{u}_{(CIP)} \quad \text{and} \tag{1}$$

$$\vec{u}^{*}_{CIP} = (1-\lambda_{CIP})\,\vec{u}_{(MPS)} + \lambda_{CIP}\,\vec{u}_{CIP}\,. \tag{2}$$

Here, u_{MPS} is velocity defined in terms of particle coordinates, given by the advection part of MPS, and $u_{(MPS)}$ is velocity interpolated in terms of grid coordinates; u_{CIP} is velocity defined in terms of grid coordinates, given by the advection equations of CIP; and $u_{(CIP)}$ is velocity interpolated in terms of

particle coordinates. The interpolation functions between particle coordinates and grid coordinates, and the weight function are written as

$$\vec{u}_{(MPS)} = \frac{\sum_{i \neq j} \vec{u}_{MPS}\, W(R_{ij})}{\sum_{i \neq j} W(R_{ij})}, \tag{3}$$

$$\vec{u}_{(CIP)} = \frac{\sum_{i \neq j} \vec{u}_{CIP}\, W(R_{ij})}{\sum_{i \neq j} W(R_{ij})} \quad \text{and} \tag{4}$$

$$W(R_{ij}) = \begin{cases} \dfrac{R_e}{R_{ij}} - 1 & \left(R_{ij} \le R_e\right) \\ 0 & \left(R_{ij} > R_e\right) \end{cases}, \tag{5}$$

where R_{ij} is the distance between i th particle and j th grid, and R_e is an effective range defined as 1.0 to 1.5 cells. In Eqs. (1) and (2), λ is a function for switching the velocities given by MPS or CIP and is defined in terms of the particle number density and the distance (defined by the number of cells shown in Fig. 3) from a free surface; λ_{MPS} and λ_{CIP} are given as

$$\lambda_{MPS} = \begin{cases} 0 & (\delta^{(i)} < \delta^{(i)}_{\min}) \\ (\delta^{(i)} - \delta^{(i)}_{\min}) / (\delta^{(i)}_{\max} - \delta^{(i)}_{\min}) & (\delta^{(i)}_{\min} \le \delta^{(i)} \le \delta^{(i)}_{\max}) \\ 1 & (\delta^{(i)} > \delta^{(i)}_{\max}) \end{cases}, \tag{6}$$

$$\lambda_{CIP} = \lambda_{MPS}\,(1-\beta), \tag{7}$$

where,

$$\beta = \theta_{CIP}\,\beta^{(1)} + (1-\theta_{CIP})\beta^{(2)}, \tag{8}$$

$$\beta^{(i)} = \sum_{i \neq j} N^{(i)} \Big/ N_0 \quad \text{and} \tag{9}$$

$$N^{(i)} = \sum_{i \neq j} W(R_{ij})^{(i)}. \tag{10}$$

Here, θ_{CIP} is the volume fraction of liquid calculated in CIP (θ_{CIP} is 0 in air, and θ_{CIP} is 1 in fuel). $N^{(i)}$ is particle-number density, where i (i = 1 or 2) means the kind of fluid; in this study, fluid 1 (i = 1) means the air and fluid 2 (i = 2) means the fuel. N_0 is the particle-number density calculated by using the particle distribution at the start of computation.

Figure 2 shows a simulation model of the liquid-film breakup in a collision jet. Fuel goes thorough a pass under the plunger rod and then enters the nozzles. Liquid columns are formed at the nozzle outlets and then make a collision jet. After the liquid columns collide, a liquid film is formed, the tip of the liquid film breaks up into ligaments, and then the ligaments break up into the droplets. The free surfaces calculated in CIP disappear due to numerical diffusion if they become close to the sizes of the computational grids, while the particles in MPS are left. In this study, particles used in MPS were generated within the nozzles, the liquid column, and the liquid film. (When the particles were generated only within the nozzle, the smooth liquid-film was not formed due to scattering particles.) The particles were generated in the region where θ_{CIP} was more than 0.5 and the particle density (= [particle number density] / [initial particle number density]) was less than 0.97. If the threshold of θ_{CIP} was set close to 1.0, the convergence of computation became unstable. The threshold of 0.97 of the particle density was the same as that of the pressure boundary condition on the free surface in MPS. The particles outside the computational region were removed. Furthermore, different time steps were used in CIP and MPS for stable convergence of computation; the ratio was set to 20, that is, the advection velocities in MPS were modified every 20 time-steps with those in CIP.

The boundary condition between MPS and CIP was defined as only the advection velocity, and the particle pressure in MPS was used to keep a uniform distance between particles; pressure was set to zero if the particle density (= [particle number density] / [initial particle number density]) was less than 0.97. In Fig. 2, the particle pressure on the free surfaces (and, in some cases, particles inside the fuel) is set to zero.

Figure 3 expands region A from Fig. 2 to define distance from an interface. Here, $\delta^{(i)}$ (i =1, 2) is distance (defined as the number of cells) from a free surface, and $\delta^{(i)}$ is positive in the arrow direction. The red line is an interface between fluids 1 and 2 in CIP, and the interface is defined as 0.5 of volume fraction of liquid in CIP. The distance from the interface is defined as the number of cells from the red line (in 3D simulation, the red line is a surface). The distance at a particle position is given as

$$D_{(MPS)} = \frac{\sum_{i \neq j} D_{CIP}\, W(R_{ij})}{\sum_{i \neq j} W(R_{ij})}. \tag{11}$$

Here, D_{CIP} is the distance defined in CIP (D_{CIP} is defined at the center of cells), and $D_{(MPS)}$ is the distance interpolated in terms of particle coordinates. Advection velocity near free surfaces was calculated by MPS (δ is from 0 to δ_{min}), and that outside free surfaces was calculated by CIP (δ is more than δ_{max}).

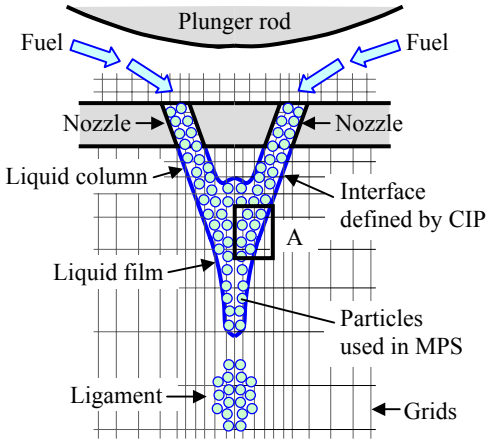

Fig. 2 Simulation model for liquid-film breakup near nozzle outlets

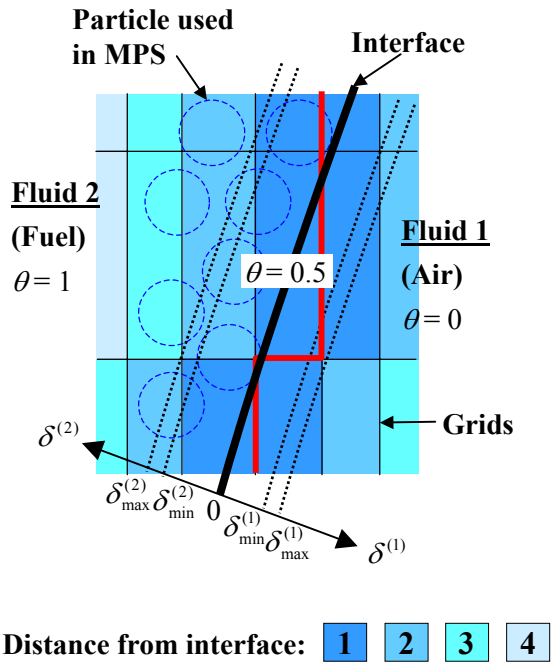

Fig. 3 Definition of distance from interface (expansion of region *A* in Fig. 2).

In the range between δ_{min} and δ_{max}, the advection velocity was calculated by combining the advection velocities given by MPS and CIP. In eqs. (1) and (2), the advection velocity in MPS is used in the range from 0 to δ_{min}, and the advection velocity in CIP is used outside δ_{max}. (When particle density β is close 1, the advection velocity in MPS is used in all cases.) In the range between δ_{min} and δ_{max}, the advection velocity is interpolated between those in CIP and MPS. The difference between $\delta_{\min}$ and $\delta_{\max}$ was set to 0.5 (half a cell). If a larger difference between $\delta^{(i)}_{\min}$ and $\delta^{(i)}_{\max}$ had been used, numerical stability would have improved; however, the interface of the free surface would have been smoothed out more.

In this study, to shorten the computational time, particles only for fluid 2 (fuel) in Fig. 3 were simulated, and particles for air were neglected (in other words, the single-phase particle-model was used; the two-phase particle-model was not used). Surface tension was calculated by MPS. In the calculation, a surface-tension model developed by Kondo et al. [13] was used; the model has good convergence in computation because the surface tension is calculated by attractive force based on a potential force. The effective radius for calculating the surface tension was set to 2.2 times larger than the initial particle distance.

Air/Fuel mixture simulation Fuel-droplet behavior in the air/fuel mixture region was simulated by DDM [10]; a DDM-droplet is a group of droplets injected under the same conditions in terms of velocity, diameter, and time. The DDM-droplet was defined as a sphere, and the motion of the DDM-droplet was calculated by using the following equations:

$$\frac{d\vec{u}_d}{dt} = \frac{3\rho_a}{4\rho_d d_d} C_D \left|\vec{u}_a - \vec{u}_d\right|\left(\vec{u}_a - \vec{u}_d\right), \tag{12}$$

where

$$C_D = \left(0.63 + 4.8/\sqrt{\mathrm{Re}_d}\right)^2 \quad \text{and} \tag{13}$$

$$\mathrm{Re}_d = \left|\vec{u}_a - \vec{u}_d\right| d_d \rho_a / \mu_a \ . \tag{14}$$

Here, subscripts *d* and *a* represent droplets and air, respectively. The injection conditions (namely, velocity and diameter distributions of the DDM droplets) were defined in accordance with the results of the liquid-film-breakup simulation, and the data-sampling region was set within a few millimeters of the injector outlet. The airflow was simulated by a finite volume method, and turbulence flow was simulated by quasi-direct numerical simulation on the basis of Kawamura and Kuwahara's scheme (third-order resolution) [14].

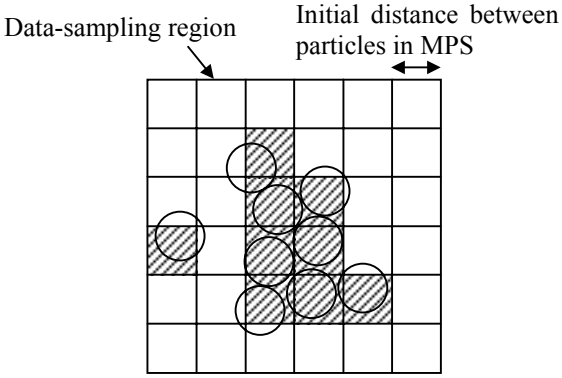

Fig. 4 Calculation of velocity and diameter distributions of droplets in data-sampling region.

Combination of liquid-film breakup and air/fuel mixture simulations The injection conditions of DDM were calculated from the particle distribution simulated in MPS for the liquid-film-breakup simulation. The particles were assigned to uniform cubic grids within the data-sampling region; in particular, the size of the cubic grids was set to the initial distance between particles in MPS (see Fig. 4). The particle distribution (shown by the hatched region) was used to calculate the velocity and diameter distributions of droplets. In the case of MPS, a droplet was formed from a group of particles, so isolated particles had no physical meaning. Accordingly, droplets formed from more than four particles were used to calculate the velocity and diameter distributions.

The flow rate of fuel was calculated from the mass flow rate *q* at the inlet boundary used in CIP and the injection time T_{shot}; the number of DDM droplets was calculated by using the following equation:

$$N_p = \frac{\int_0^{T_{shot}} q dt}{N_{shot} \sum_{i=1}^{n} (\rho V_i)} . \quad (15)$$

Here, V_i is volume of i th droplet, ρ is density of the droplet, n is the number of droplets in the data-sampling region, and N_{shot} is the number of the data sampling. Calculating the numerator in Eq. (15) needs a long computation time. In this study, the data was sampled under the steady flow conditions, and then the numerator in Eq. (15) was simplified as

$$\int_0^{T_{shot}} q dt \approx \rho T_{shot} \int u_{inlet} dA_{inlet} . \quad (16)$$

Here, u_{inlet} is velocity at the inlet in CIP and A_{inlet} is the inlet area.

COMPUTATIONAL MODEL

Figure 5 shows grids (a) the computational grids used for the liquid-film-breakup simulation and (b) the grids for the air/fuel mixture simulation. Figure 5(a) consists of hexahedral grids with 204,950 cells. In particular, a geometry half the size of the original was used in the simulation, six nozzles (twelve nozzles in the original model) were assigned at the end of the inner flow path, and the size of the air region was set to 3 mm below the nozzles. The six nozzles in Fig. 5 generated three pairs of collision jets; each dashed-line circle in Fig. 5(a) shows a pair of nozzles. The bottom and the side boundaries except the symmetric boundary were defined as the outlet boundary. Figure 5(b) consists of uniform cubic grids with one million cells. The grid generator used for the air/fuel mixture simulation was based on the Cartesian-grid method, so a complex geometry of grids was generated in a short time from CAD data. However, the simple geometry of grids shown in Fig. 5(b) was used to verify the present simulation model. In Fig. 5(b), an injection point was located at the top-center position of the computational region, and the size of the air region was set to 100 mm; the minimum size of computational grids was 1 mm. All boundaries were defined as walls. The fuel pressure at the inlet boundary in Fig. 5(a) was 0.4 MPa, and the pressure in the air region was 0.1 MPa. The air and fuel densities were 1.18 kg/m^3 and 783 kg/m^3, and their viscosities were 1.86×10^{-5} Pa·s and 8.46×10^{-4} Pa·s, respectively. The surface tension was set to 28.0×10^{-3} N/m. About 20,000 particles were used in MPS (initial distance of particles was 22.9 μm). The time steps in CIP and MPS were 1.0×10^{-7} s and 2.0×10^{-6} s respectively; the advection velocities in both methods were modified every 20 steps in CIP. The time step in air/fuel mixture simulation was 6.0×10^{-6} s. The CPU time for one case in the liquid-film breakup simulation was about 8 hours with a PC of 3.0 GHz CPU, and that in the air/fuel mixture simulation was about 5 hours with a PC of 2.66 GHz CPU.

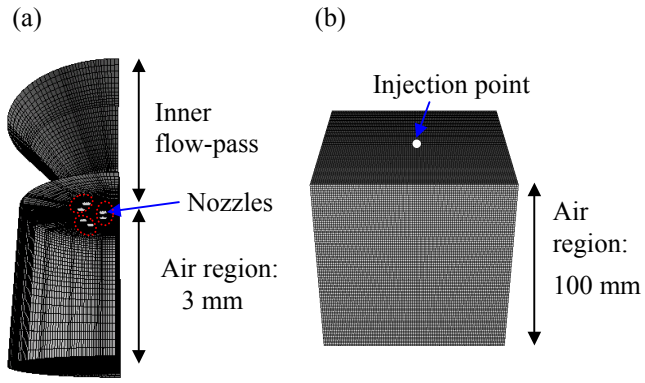

Fig. 5 Computational grids: (a) grids for liquid-film breakup simulation (204,950 cells. half size of original geometry), and (b) grids for air/fuel mixture simulation (1,000,000 cells).

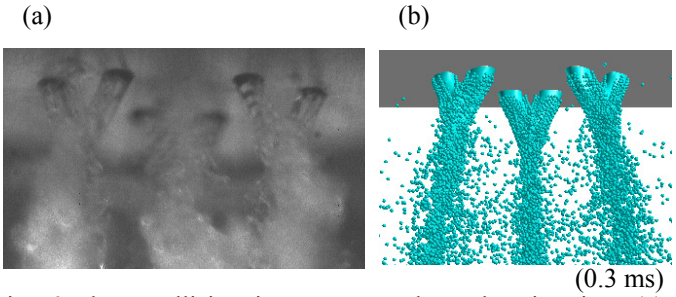

Fig. 6 Three collision jets near nozzle outlets in Fig. 5(a) viewed from left: (a) measurement and (b) simulation.

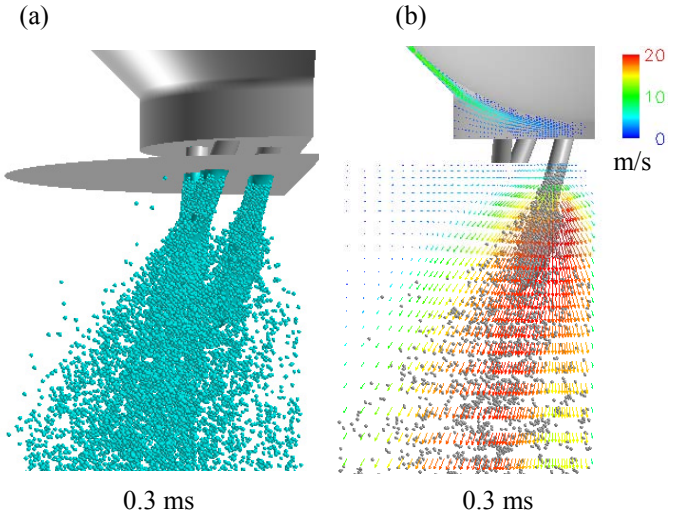

Fig. 7 Collision jets near nozzle outlets viewed from front in Fig. 5(a): (a) fuel distribution, and (b) velocity distribution.

RESULTS AND DISCUSSION

Figure 6 compares the simulated liquid-film breakup with the measured breakup: (a) the measurement and (b) the simulation. Figure 6 shows Fig. 5(a) from the left and snap shots in a steady state of the collision jets. The behavior of the collision jets in the simulation (0.3 ms) agrees well with the measured behavior. Figure 7 shows the fuel distribution in Fig. 5(a) from the front. The fuel distribution is represented with particles in MPS; the liquid films, ligaments, etc. are formed by groups of particles. In Fig. 7(a), the three collision jets form one beam that advances to the bottom left. (In the original model, the beam in the right half in Fig. 7(a) advances to the bottom right, that is, two beams was formed in the spray of the original model.) Figure 7(b) shows the velocity distribution (calculated in CIP) in the center plane; the fuel goes through the pass under the plunger rod, and velocity with high speed (about 20 m/s) is generated in the liquid film formed by two liquid columns colliding (the maximum velocity was 24 m/s within the nozzle).

Table 1 compares spray properties between the measurement and the simulation; the jet angle (at 3.75 ms, details are shown in Fig. 9) in the measurement was 60°, and that in the simulation was 64°. The flow rate in the simulation was 7 % larger than that in the measurement, and the mean diameter, D_{32}, in the simulation was 35 % larger than that in the measurement. The mean diameter, D_{32}, is defined as

$$D_{32} = \frac{\sum_i n_i d_i^3}{\sum_i n_i d_i^2} . \quad (17)$$

Here, d_i is diameter of i th droplet, and n_i is number of particles with the diameter d_i. The D_{32} in the simulation depends on the initial distance between particles, and relationship between D_{32} and the initial distance between particles will be studied in future work.

In Fig. 7(a), free surfaces of the liquid film, ligaments, and droplets are represented as groups of particles. In some cases, it was difficult to imagine the shapes of the free surfaces. Figure 8 shows the free surfaces visualized by ray tracing [15] from the particle distributions. In (a), six pairs of collision jets are shown, Fig. 5(a) is viewed from the front, and the simulation results in the left half of Fig. 8(a) were copied to the right half. In (b), the center collision jet among the three collision jets in the right-half side of Fig. 8(a) is shown. The liquid film is visualized as a continuum body, and its breakup into regiments is visualized realistically. The tip of the liquid film breaks up into ligaments, and the ligaments break up into droplets. The standard time (0 ms) is set to the time when the liquid columns appeared from the nozzle outlets.

Table 1 Comparison of spray properties in the simulation with those in the measurement.

Jet angle (at 3.75 ms)	Measurement	60°
	Simulation	64°
Difference in flow rate	+ 7 %	
Difference in mean diameter, D_{32}	+ 35 %	

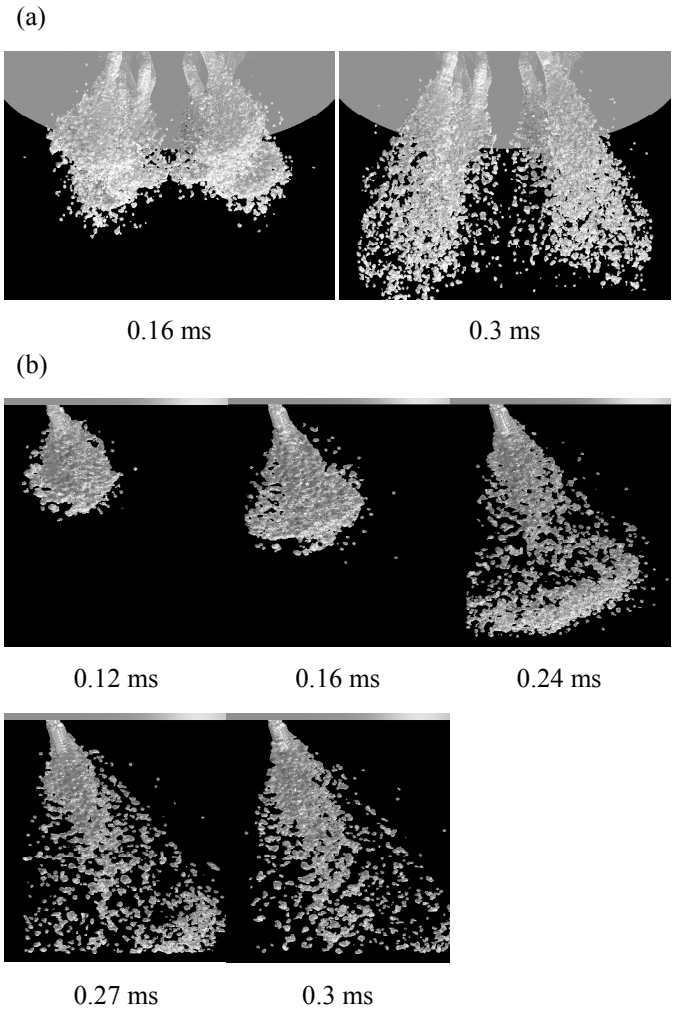

Fig. 8 Liquid-film breakup visualized by ray tracing. (a) six collision jets in Fig. 5(a) viewed from front. Spray data in right half in Fig. 7(a) was copied from that in left half. (b) liquid-film breakup of a collision jet.

Figure 9(a) shows snap shots from different times of the measured air/fuel mixture, and (b) and (c) show simulation results under different injection conditions for DDM droplets; (b) the diameter and the velocity distributions were given from the liquid-film breakup simulation (by MPS), and (c) the diameter distribution was given by Nukiyama-Tanazawa's theory (the mean diameter was calculated by using the results of the liquid-film breakup simulation), and the velocity distribution was given from the liquid-film breakup simulation (by MPS).

The calculated velocity and diameter distributions in the data-sampling region were given in half the size of the original geometry (see Fig. 5(a)); accordingly, the velocity and diameter distributions were copied on the right side of Fig. 5(a) symmetrically. Figure 9 shows Fig. 5(a) from the front; the fuel spray from 12 nozzles spreads in two directions.

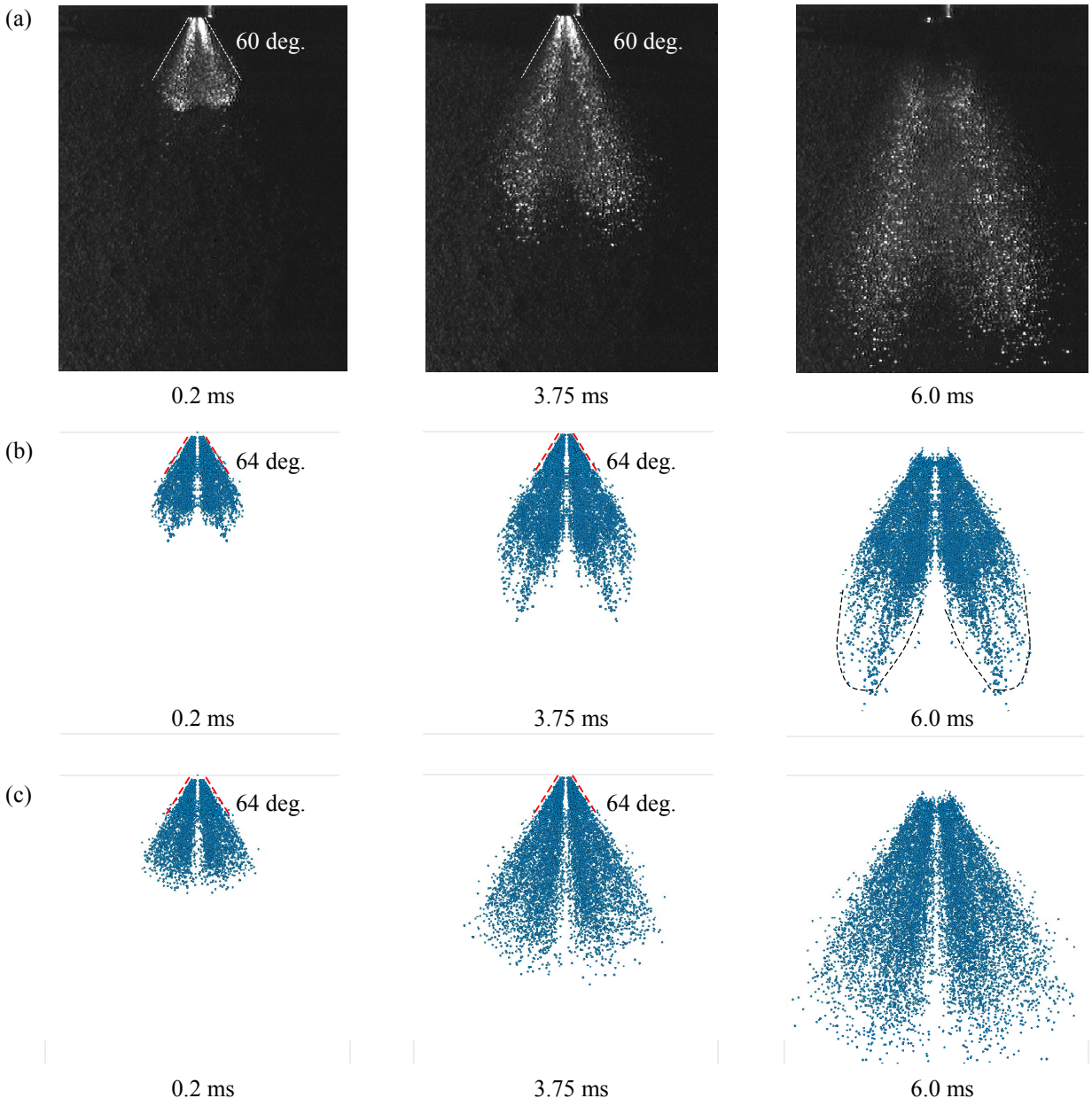

Fig. 9 Air/fuel mixtures of collision injector. (a) measurements. Simulations under different injection conditions; (b) diameters: MPS, velocities: MPS; and (c) diameters: Nukiyama-Tanazawa's theory, velocities: MPS.

The behavior of the air/fuel mixture in (b) qualitatively agrees with that of the measurements with time; the simulated results show two leading edges at the bottom of the spray, but the lengths of leading edges are a little longer than those in measurements, while the simulation results in (c) show ambiguous leading edges at the bottom of sprays. The simulated jet angle was also compared with the measured one; the angle was defined at the time of 3.75 ms by using the spray profiles at the tops of sprays. The simulated angle was 64 degrees, larger than the 60 degrees of the measurement.

Figure 10 compares the air/fuel mixture under three injection conditions. Here, in (d), a new injection condition is added to those in Fig. 9: the diameter distribution was given by Nukiyama-Tanazawa's theory and the velocity-distribution was given as the uniform velocity (mean velocity) calculated by using the results of the liquid-film breakup simulation. The shape of the leading edge in (d) is almost the same as that in (c), and the diameter distribution under the injection conditions was found to affect the shape of the leading edge; the spray in (b) includes relatively large droplets, which pull surrounding air with other relatively small droplets, and then the leading edges are formed.

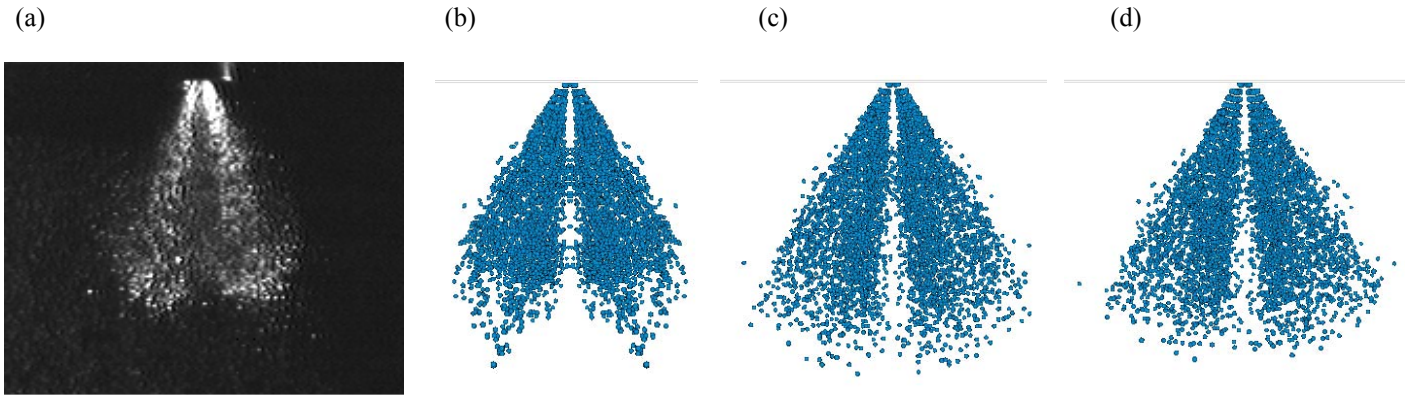

Fig. 10 Comparison of air/fuel mixtures under different injection conditions (at 2.25 ms): (a) measurement, (b) diameters: MPS, velocities: MPS, (c) diameters: Nukiyama-Tanazawa's theory, velocities: MPS, and (d) diameters: Nukiyama-Tanazawa's theory, velocities: uniform velocity (mean velocity in MPS).

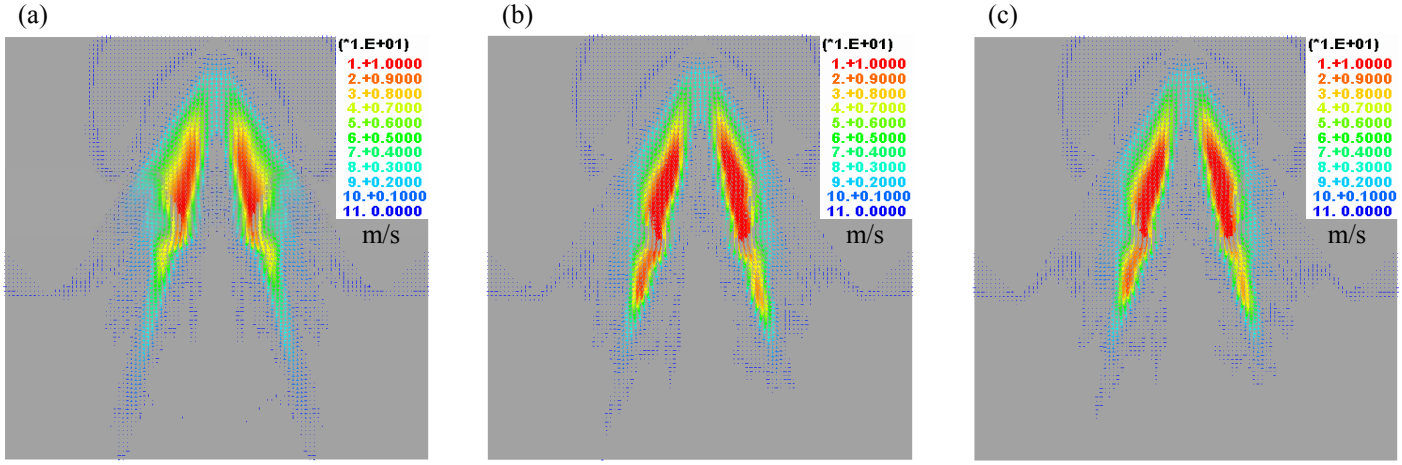

Fig. 11 Velocity distributions in air/fuel mixture regions (at 6.0 ms);(a) diameters: MPS, velocities: MPS, (b) diameters: Nukiyama-Tanazawa's theory, velocities: MPS, and (c) diameters: Nukiyama-Tanazawa's theory, velocities: uniform velocity (mean velocity in MPS).

Figure 11 shows velocity distributions in the air/fuel mixture region at 6.0 ms under the three injection conditions: (a) the diameter and the velocity distributions were given from the liquid-film breakup simulation (by MPS); (b) the diameter distribution was given by Nukiyama-Tanazawa's theory (the mean diameter was calculated by using the results of the liquid-film breakup simulation) and the velocity distribution was given from the liquid-film breakup simulation (by MPS); and (c) the diameter distribution was given by Nukiyama-Tanazawa's theory and the velocity-distribution was given as the uniform velocity (mean velocity) calculated by using the results of the liquid-film breakup simulation. In Fig. 11(a), the velocity in the part of the leading edge is higher than those in (b) and (c); the velocity was formed by relatively large droplets in the spray. The velocity distributions in (b) and (c) were almost the same.

SUMMARY

Fuel sprays formed by collision jets for automobile engines were simulated by combining the liquid-film breakup simulation and the air/fuel mixture simulation. The liquid-film breakup was simulated by a particle method, and the fuel-droplet behavior in the air/fuel mixture region was simulated by a discrete droplet model (DDM). The results of the study are as follows:

1. The spray properties in the simulation were compared with those in the measurements. The jet angle in the measurements was 60°, and that in the simulation was 64°. The flow rate in the simulation was 7 % larger than that in the measurements, and the mean diameter, D_{32}, in the simulation was 35 % larger than that in the measurement.
2. The effects were studied of DDM-droplet injection conditions on the air/fuel mixture. Three injection conditions were studied: (a) the diameter and the velocity given by the liquid-film breakup simulation, (b) the diameters given by Nukiyama-Tanazawa's theory and the velocities given by the liquid-film breakup simulation, and (c) the diameters given by Nukiyama-Tanazawa's theory and the velocities given by uniform mean-velocity. The behavior of the air/fuel mixture with (a) qualitatively agreed with that of the measurements; the simulation with (a) showed two leading edges at the bottom of sprays that were the same as the measurements, while the simulations with (b) and (c) showed no leading edge at the bottom of sprays. The diameter distribution under the injection condition was found to affect the shape of the leading edge.

Our method combining the liquid-film breakup and the air/fuel mixture was found to be useful in the fuel-spray simulation for automobile engines.

REFERENCES

[1] Hirt, C. W. and Nichols, B. D., 1981, "Volume of fluid (VOF) method for the dynamics of free boundaries," Journal of Computational Physics, 39, pp. 201-225.

[2] Sussman, M. Smereka, P., and Osher, S., 1994, "A Level Set Approach for Computing Solutions to Incompressible Two-Phase Flow," Journal of Computational Physics, 114, pp. 146-159.

[3] Yabe, T. and Aoki, T., 1996, "A Dream to Solve Dynamics of All Materials Together," International Conference on High-performance Computing in Automotive Design, Engineering, and Manufacturing, Oct. 7-10, 1996, Paris, France, pp. 2105-2108.

[4] Tanguy, S., et al., 2004, "Developpement D'une Methode Level Set Pour Le Suivi D'interfaces et Applications," Advances in the Modeling Methodologies of Two-phase flows, Lyons, France, Paper No. 13.

[5] Tanguy and Berlemond, 2005, "Application of a level set method for simulation of droplet collisions," International Journal of Multiphase Flow, 31, pp. 1015-1035.

[6] Pan, Y. and Suga, K., 2004, "Direct Simulation of Water Jet into Air," 5th International Conference on Multiphase Flow, ICMF'04, Paper No. 377.

[7] Ishii, E., Ishikawa, T., and Tanabe, Y., 2006, "Hybrid Particle/Grid Method for Predicting Motion of Micro- and Macro-free Surfaces," Transaction of ASME, Journal of Fluids Engineering, 128, pp. 921-930.

[8] Ishii, E., Ishikawa, T., and Tanabe, Y., 2007, "Simulation of Liquid Jet Breakup of A Swirl-type Fuel Injector for Automobile Engines," Proceedings of ASME FEDSM'07, Paper No. FEDSM2007-37010.

[9] Koshizuka, S. and Oka, Y., 1996, "Moving-particle Semi-implicit Method for Fragmentation of Incompressible Fluid," Nucl. Sci. Eng., 123, pp. 421-434.

[10] Amsden, A. A., Ramshaw, J. D., O'Rourke, P. J. and Dukowicz, J. K., 1985, "KIVA; A Computer Program for Two- and Three-Dimensional Fluid Flows with Chemical Reactions and Fuel Sprays", Los Alamos National Laboratory Report, LA-10245-MS.

[11] Ishii, E., Yasukawa, Y., Sukegawa, Y. and Yamada, H., A Fuel-spray Simulation considering Fuel-jet Breakup near Fuel Injector and Composition of Air/fuel Mixture, Proceedings of the ASME 2009 International Mechanical Engineering Congress & Exposition, CD-ROM, Paper No. IMECE2009-12380 (2009).

[12] Sukegawa, Y., Nogi, T., Kihara, Y., and Furuhashi, T., 2000, "Numerical Simulation for Mixture Formation and Combustion in Direct Fuel Injection Gasoline Engines," Seoul 2000 FISITA World Automotive Congress F2000A139.

[13] Kondo, M., Koshizuka, S., Suzuki, K. and Takimoto, M., 2007, "Surface Tension Model using Inter-Particle Force in Particle Method," Proceedings of ASME FEDSM'07, Paper No. FEDSM2007-37215.

[14] Kawamura, T. and Kuwahara, K., 1984, "Computation of High Reynolds Number Flow Around

a Circular Cylinder with Surface Roughness," AIAA Paper, 84-0340.
[15] http://www.povray.org

